General properties on applying the principle of minimum sensitivity to high-order perturbative QCD predictions

Yang Ma, Xing-Gang Wu,* Hong-Hao Ma, and Hua-Yong Han

Department of Physics, Chongqing University, Shapingba, Chongqing 401331, People's Republic of China and Institute of Theoretical Physics, Chongqing University, Shapingba, Chongqing 401331, People's Republic of China

(Received 31 December 2014; published 12 February 2015)

As one of the key components of perturbative QCD theory, it is helpful to find a systematic and reliable way to set the renormalization scale for a high-energy process. The conventional treatment is to take a typical momentum as the renormalization scale, which assigns an arbitrary range and an arbitrary systematic error to pQCD predictions, leading to the well-known renormalization scheme and scale ambiguities. As a practical solution for such a scale setting problem, the "principle of minimum sensitivity" (PMS) has been proposed in the literature. The PMS suggests to determine an optimal scale for the pQCD approximant of an observable by requiring its slope over the scheme and scale changes to vanish. In this paper, we present a detailed discussion on general properties of the PMS by utilizing three quantities $R_{e^+e^-}$, R_τ and $\Gamma(H \to b\bar{b})$ up to four-loop QCD corrections. After applying the PMS, the accuracy of pQCD prediction, the pQCD convergence, the pQCD predictive power, etc., are discussed. Furthermore, we compare the PMS with another fundamental scale setting approach, i.e. the principle of maximum conformality (PMC). The PMC is theoretically sound, which follows the renormalization group equation to determine the running behavior of the coupling constant and satisfies the standard renormalization group invariance. Our results show that PMS does provide a practical way to set the effective scale for high-energy process, and the PMS prediction agrees with the PMC one by including enough high-order QCD corrections, both of which shall be more accurate than the prediction under the conventional scale setting. However, the PMS pQCD convergence is an accidental, which usually fails to achieve a correct prediction of unknown high-order contributions with next-to-leading order QCD correction only, i.e. it is always far from the "true" values predicted by including more high-order contributions.

DOI: 10.1103/PhysRevD.91.034006 PACS numbers: 12.38.Bx, 12.38.Aw, 11.15.Bt

I. INTRODUCTION

According to the renormalization group (RG) invariance [1–6], a physical observable should not depend on any "unphysical" choices. In other words, the RG invariance indicates that the dependence of an observable on the renormalization scheme and scale should vanish. However, for fixed-order pQCD approximations, the renormalization scheme and scale dependence from both the running coupling and the corresponding expansion coefficients at the same order do not exactly cancel. To deal with a fixed-order calculation, one usually takes the renormalization scale as the typical momentum transfer of the process, or a value to minimize the contributions of large loop diagrams, and varies it over a certain range to ascertain its uncertainty. This conventional scale setting procedure leads to well-known renormalization scheme and scale ambiguities and assigns an arbitrary range and an arbitrary systematic error to fixed-order pQCD predictions. To solve such renormalization scheme and scale ambiguities, it is helpful to find a general way to set the optimal scale and hence the optimal running behavior of the strong coupling constant for any processes via a process-independent and systematic way, cf. a recent review on QCD scale setting [7].

To compare with the conventional scale setting, it has been suggested by Stevenson [8,9] that one can achieve a good prediction for an observable by requiring its pQCD approximant to be minimum sensitive to the variations of those unphysical parameters. This treatment is called as the principle of minimum sensitivity (PMS) [8–10]. The PMS admits that different scheme and scale choices do lead to theoretical uncertainties; however the true prediction of an observable can only be achieved by using optimal scheme and scale. The scheme dependence of the PMS predictions have been analyzed in Refs.[11,12]. It is noted that the PMS satisfies local RG invariance [13], which provides a practical approach to systematically fix the optimal scheme and scale for a high-energy process. It has been noted that after applying the PMS, the pQCD prediction does show a fast steady behavior over the scheme and scale changes. As an example, it has been applied to study the fixed-point behavior of the coupling constant at the low-energy region [14,15].

On the other hand, it has also been observed that the PMS does not satisfy the RG properties such as symmetry, reflexivity, and transitivity [16]. So the relations among different physical observables depend on the choice of

*wuxg@cqu.edu.cn

intermediate renormalization scheme, leading to residual scheme dependence. Moreover, the predicted PMS scale for three-jet production via e^+e^- annihilation cannot yield correct physical behavior at the next-to-leading order (NLO) level, i.e. it anomalously rises without bound for small jet energy [17,18]. There are even doubts on the usefulness of the PMS [19]. All those discussions indicate the necessity of further careful studies on theoretical principles underlying the PMS and on applications to more high-loop examples.

Great improvements on understanding the PMS procedures and on applying the PMS scale setting to higher perturbative orders other than the NLO level have recently been achieved in Ref. [20]. In recent years, there has been much progress on studying the two-loop and higher QCD corrections. For examples, the quantities $R_{e^+e^-}$, R_τ and $\Gamma(H \to b\bar{b})$ have been calculated up to four-loop level under the $\overline{\rm MS}$ scheme [21–24]. With all those developments, it is possible to make a detailed discussion on general properties of the PMS, and to show to what degree it can be applied. For the purpose, we shall present the PMS predictions for $R_{e^+e^-}$, R_τ and $\Gamma(H \to b\bar{b})$ up to four-loop level. General PMS properties, such as the accuracy of the pQCD prediction, the convergence of the perturbative series, the predictive power of pQCD theory, etc., shall be discussed via comparing the predictions with those under the conventional scale setting.

Recently, another well-known scale setting approach, i.e. the Brodsky-Lepage-Mackenzie approach suggested by Brodsky *et al.* [25], has been developed into a fundamental one, i.e. the principle of maximum conformality (PMC) [26–32]. Unlike the PMS scale setting, the PMC states that we should determine different optimal scales for the high-energy process under different schemes, and the final predictions are independent on the scheme choices due to commensurate scale relations [33] and also the scheme independence of a conformal series. The running behavior of the coupling constant is governed by the RG equation [34–40]. Inversely, the PMC states that the optimal behavior/scale of the coupling constant can be achieved by using the β terms in perturbative series. The PMC follows standard RG invariance and satisfies all RG properties [16]. When one applies the PMC, the scales of the coupling constant are shifted at each order such that no contributions proportional to the QCD β function remain. The resulting pQCD series is thus identical to a scheme-independent conformal series. Since the resulting series is free of divergent renormalon terms [41,42], the pQCD convergence can be naturally improved. The PMS and PMC scale settings have quite different starting points and their predictions usually have a quite different perturbative nature; it is thus helpful to present a detailed comparison of the PMS predictions with the PMC ones.

The remaining parts of the paper are organized as follows. In Sec. II we first present a short review on local RG invariance that underlies the PMS; then we present the PMS formulas up to high-perturbative orders. A tricky way to derive the PMS RG invariants at high orders is shown in the Appendix. In Sec. III we investigate the PMS properties based on three quantities $R_{e^+e^-}$, R_τ and $\Gamma(H \to b\bar{b})$ up to four-loop level. In Sec. IV we present a detailed comparison of the PMS and PMC via the quantity $R_{e^+e^-}$. Section V is reserved for a summary.

II. CALCULATION TECHNOLOGY FOR THE PMS SCALE SETTING

Conventionally, the running behavior of the strong coupling constant is controlled by the following $\beta^{\mathcal{R}}$ function or the RG equation,

$$\beta^{\mathcal{R}} = \mu^2 \frac{\partial}{\partial \mu^2}\left(\frac{\alpha_s^{\mathcal{R}}(\mu)}{4\pi}\right) = -\sum_{i=0}^{\infty} \beta_i^{\mathcal{R}} \left(\frac{\alpha_s^{\mathcal{R}}(\mu)}{4\pi}\right)^{i+2}, \quad (1)$$

where μ stands for the renormalization scale, and the superscript $\mathcal{R}$ stands for an arbitrary renormalization scheme (usually taken as the $\overline{\rm MS}$ scheme). For convenience and without introducing any confusion, we shall omit the superscript $\mathcal{R}$ in the following formulas. The first two β terms, $\beta_0 = 11 - \frac{2}{3}n_f$ and $\beta_1 = 102 - \frac{38}{3}n_f$, are scheme independent, where n_f is the number of active flavors, while the β_n terms with $(n \geq 2)$ are scheme dependent [36–40]. The scheme dependence/transformation for high-order β terms has been discussed in Refs. [43–45].

It is convenient to use $\tau = \ln(\mu^2/\tilde{\Lambda}^2_{\rm QCD})$ and $\beta_{n\geq 2}$ to label a particular choice of renormalization scale and renormalization scheme [8]. Here $\tilde{\Lambda}_{\rm QCD}$ is the reduced asymptotic scale, which is defined as

$$\tilde{\Lambda}_{\rm QCD} = \left(\frac{\beta_1}{\beta_0^2}\right)^{-\beta_1/2\beta_0^2} \Lambda_{\rm QCD}. \quad (2)$$

We can study the scale and scheme dependence of the pQCD predictions via the extended RG equations [8,46].

A. Local RG invariance and the PMS

As an illustration of local RG invariance, we deal with the perturbative approximant (ϱ_n) for an arbitrary physical observable ϱ, which can be written as

$$\varrho_n(Q) = \mathcal{C}_0(Q) a_s^p(\mu) + \sum_{i=1}^{n} \mathcal{C}_i(Q,\mu) a_s^{i+p}(\mu), \quad (3)$$

where Q is the experimental scale at which it is measured, $a_s = \alpha_s/\pi$, and p is the power of coupling constant associated with tree-level term. The calculation of the coefficients $\mathcal{C}_i$ involves ultraviolet divergences which must be regulated and removed by a renormalization procedure. At the finite order, the pQCD predictions depend on the choice of renormalization scheme and scale, which indicates that

$$\partial\varrho_n/\partial(\mathrm{RS}) = \mathcal{O}(a_s^{p+n}), \tag{4}$$

where RS stands for the scheme or scale parameter, respectively. Equation (4) shows the self consistency of a perturbation theory, i.e. the N^n-leading order (LO) approximate ϱ_n must agree to $\mathcal{O}(a_s^{p+n})$ under different choices of scheme and scale. The tree-level coefficient $\mathcal{C}_0$ is scheme and scale independent; we set its value to be 1 in later calculations. When $\mathcal{C}_0 \neq 1$, the results can be obtained via the transformation, $\mathcal{C}_i(Q,\mu) \to \mathcal{C}_i'(Q,\mu) = \mathcal{C}_i(Q,\mu)/\mathcal{C}_0$.

As mentioned in the introduction, there are renormalization scheme and scale ambiguities for the fixed-order pQCD approximant ϱ_n. The PMS suggests to eliminate such scheme and scale ambiguities by finding optimal scheme and optimal scale of the process, which can be achieved by requiring ϱ_n to satisfy the following equations [8,20]:

$$\frac{\partial\varrho_n}{\partial\tau} = 0, \tag{5}$$

$$\frac{\partial\varrho_n}{\partial\beta_m} = 0. \qquad (m = 2,\ldots,n). \tag{6}$$

They can be further written as

$$\frac{\partial\varrho_n}{\partial\tau} = \left(\frac{\partial}{\partial\tau}\bigg|_{a_s} + \beta(a_s)\frac{\partial}{\partial(a_s/4)}\right)\varrho_n = 0, \tag{7}$$

$$\frac{\partial\varrho_n}{\partial\beta_m} = \left(\frac{\partial}{\partial\beta_m}\bigg|_{a_s} - \beta(a_s)\int_0^{a_s/4} d\left(\frac{a_s'}{4}\right)\frac{(a_s'/4)^{m+2}}{[\beta(a_s')]^2}\frac{\partial}{\partial(a_s/4)}\right)\varrho_n = 0, \qquad (m = 2,3,\ldots) \tag{8}$$

where the integration in the second equations can be treated via the α_s expansion,

$$\beta(a_s)\int_0^{a_s/4} d\left(\frac{a_s'}{4}\right)\frac{(a_s'/4)^{m+2}}{[\beta(a_s')]^2} = -\frac{(a_s/4)^{j+1}}{\beta_0}\left(\frac{1}{j-1} - \frac{\beta_1}{\beta_0}\frac{j-2}{j(j-1)}\left(\frac{a_s}{4}\right) + \cdots\right).$$

The standard RG invariance states that only the physical observable $\varrho = \varrho_n|_{n\to\infty}$ agrees with those equations. Thus, using Eqs. (7)–(8) for the fixed-order approximant is theoretically unsound, and they instead introduce a kind of local RG invariance [13]. This provides the reason why the PMS does not satisfy the basic RG properties [16]. The PMS, however, provides an intuitive way to set the optimal scheme and optimal scale, and its resultant tends to be steady over the scheme and scale changes around the optimal point.

The running behavior of the strong coupling constant can be obtained via solving RG equation (1), which can be rewritten as

$$\begin{aligned}\tau &= \int_0^{a_s/4} d\left(\frac{x}{4}\right)\frac{1}{\beta^{(n)}(x)} \\ &= \frac{4}{\beta_0 a_s} + \frac{\beta_1}{\beta_0^2}\ln\left|\frac{\beta_1 a_s}{\beta_1 a_s + 4\beta_0}\right| - \Delta(a_s),\end{aligned} \tag{9}$$

where

$$\Delta(a_s) = \beta_0\int_0^{a_s/4} dx\left(\frac{1}{\beta^{(n)}(x)} - \frac{1}{\beta^{(1)}(x)}\right). \tag{10}$$

The symbol $\beta^{(n)}$ stands for the cut β function up to a_s^{n+2}. Equation (9) is the "integrated β-function equation," or simply the "int-β equation," which can be solved numerically.

In the following, we shall show how the PMS applies local RG invariance to set the optimal scale and how the RG-invariant coefficients at each order are derived.

B. PMS procedures up to high orders

For a N^n-LO pQCD approximate (3), we have to fix totally $2n+1$ variables for determining optimal scheme and optimal scale, i.e. $\tilde{a}_s, \tilde{\tau}, \tilde{\beta}_2, \ldots, \tilde{\beta}_n, \tilde{\mathcal{C}}_1, \ldots, \tilde{\mathcal{C}}_n$. Those parameters can be fixed by using n local RG equations (7)–(8), one int-β equation (9), and also n scheme- and scale-independent RG invariants from the self-consistency relation (4). To be a useful reference for applying the PMS scale setting, we take the QCD corrections up to N^3-LO level as a detailed explanation.

At the NLO level, the NLO approximate is

$$\varrho_1 = a_s^p(1 + \mathcal{C}_1 a_s).$$

The NLO approximate ϱ_1 can be calculated in an initial choice of scheme (usually the $\overline{\mathrm{MS}}$ scheme) and scale. We have three parameters $\tilde{a}_s$, $\tilde{\tau}$ and $\tilde{\mathcal{C}}_1$ to be determined.

Differentiating ϱ_1 over τ and using the self-consistency relation (4), i.e. the coefficient at the order of $\mathcal{O}(a_s^{p+1})$ should be zero, we obtain

$$\frac{\partial \mathcal{C}_1}{\partial \tau} = \frac{1}{4} p\beta_0. \tag{11}$$

Integrating it over τ, we get one RG-invariant integration constant ρ_1, which can be expressed as

$$\rho_1 = \frac{1}{4} p\beta_0 \tau - \mathcal{C}_1 = \frac{1}{4} p\beta_0 \tilde{\tau} - \tilde{\mathcal{C}}_1, \tag{12}$$

where the second equation is from the RG invariance. As a tricky point, since ρ_1 depends solitarily on Q at which the observable is measured, one can transform $\varrho_n(Q)$ as $\varrho_n(\rho_1)$. The advantage of such a transformation lies in that $\varrho_n(\rho_1)$ does not depend on $\Lambda_{\rm QCD}$, thus avoiding the uncertainties from the choice of $\Lambda_{\rm QCD}$.

From Eq. (7), we obtain the NLO local RG equation

$$p\beta_0 - [p\tilde{a}_s^{p-1} + (p+1)\tilde{\mathcal{C}}_1 \tilde{a}_s^p]\left(\beta_0 + \frac{\beta_1 \tilde{a}_s}{4}\right) = 0, \tag{13}$$

which leads to

$$\tilde{\mathcal{C}}_1 = -\frac{p\beta_1}{(p+1)(4\beta_0 + \beta_1 \tilde{a}_s)}. \tag{14}$$

Together with the NLO int-β equation

$$\tilde{\tau} = \frac{4}{\beta_0 \tilde{a}_s} + \frac{\beta_1}{\beta_0^2} \ln\left|\frac{\beta_1 \tilde{a}_s}{\beta_1 \tilde{a}_s + 4\beta_0}\right|, \tag{15}$$

we finally obtain

$$\frac{1}{\tilde{a}_s} + \frac{p\beta_1}{(p+1)(4\beta_0 + \beta_1 \tilde{a}_s)} + \frac{\beta_1}{4\beta_0} \ln\left|\frac{\beta_1 \tilde{a}_s}{\beta_1 \tilde{a}_s + 4\beta_0}\right| = \rho_1. \tag{16}$$

From those equations (14)–(16), we can derive $\tilde{\tau}$, $\tilde{\mathcal{C}}_1$, $\tilde{a}_s$, and finally get the optimized prediction for ϱ_1.

For high-order QCD corrections, we can apply similar procedures via a step-by-step way for determining all the parameters.

Using the self-consistency condition (4), the local RG invariants ρ_n can be determined via an order-by-order way. Once a ρ_n has been determined at a particular perturbative order, it shall be fixed for all high-order PMS treatment. Except for those local RG invariants, all other parameters should be redetermined when new high-order corrections are included.

At the N^2-LO level, we have five parameters to be determined, i.e. $\tilde{a}_s$, $\tilde{\tau}$, $\tilde{\beta}_2$, $\tilde{\mathcal{C}}_1$, and $\tilde{\mathcal{C}}_2$. There are two equations that can be obtained from the local RG equations $\partial\varrho_2/\partial\tau = 0$ and $\partial\varrho_2/\partial\beta_2 = 0$:

$$16(2+p)\tilde{\mathcal{C}}_2\beta_0 + 4[(1+p)\tilde{\mathcal{C}}_1 + (2+p)\tilde{\mathcal{C}}_2\tilde{a}_s]\beta_1 + [\tilde{a}_s(\tilde{\mathcal{C}}_1 + 2\tilde{\mathcal{C}}_2\tilde{a}_s) + p(1 + \tilde{\mathcal{C}}_1\tilde{a}_s + \tilde{\mathcal{C}}_2\tilde{a}_s^2)]\tilde{\beta}_2 = 0, \tag{17}$$

$$48[(1+p)\tilde{\mathcal{C}}_1 + (2+p)\tilde{\mathcal{C}}_2\tilde{a}_s]\beta_0 + \tilde{a}_s[\tilde{a}_s(\tilde{\mathcal{C}}_1 + 2\tilde{\mathcal{C}}_2\tilde{a}_s) + p(1 + \tilde{\mathcal{C}}_1\tilde{a}_s + \tilde{\mathcal{C}}_2\tilde{a}_s^2)]\tilde{\beta}_2 = 0. \tag{18}$$

At the N^3-LO level, we have seven parameters to be determined, i.e. $\tilde{a}_s$, $\tilde{\tau}$, $\tilde{\beta}_2$, $\tilde{\beta}_3$, $\tilde{\mathcal{C}}_1$, $\tilde{\mathcal{C}}_2$, and $\tilde{\mathcal{C}}_3$. There are three local RG equations that can be obtained from $\partial\varrho_3/\partial\tau = 0$, $\partial\varrho_3/\partial\beta_2 = 0$, and $\partial\varrho_3/\partial\beta_3 = 0$:

$$\begin{aligned} &64(3+p)\tilde{\mathcal{C}}_3\beta_0 + 16((2+p)\tilde{\mathcal{C}}_2 + (3+p)\tilde{\mathcal{C}}_3\tilde{a}_s)\beta_1 + 4((1+p)\tilde{\mathcal{C}}_1 + \tilde{a}_s((2+p)\tilde{\mathcal{C}}_2 + (3+p)\tilde{\mathcal{C}}_3\tilde{a}_s))\tilde{\beta}_2 \\ &+ (p + \tilde{\mathcal{C}}_1\tilde{a}_s + p\tilde{\mathcal{C}}_1\tilde{a}_s + 2\tilde{\mathcal{C}}_2\tilde{a}_s^2 + p\tilde{\mathcal{C}}_2\tilde{a}_s^2 + (3+p)\tilde{\mathcal{C}}_3\tilde{a}_s^3)\tilde{\beta}_3 = 0, \end{aligned} \tag{19}$$

$$\begin{aligned} &384[(2+p)\tilde{\mathcal{C}}_2 + (3+p)\tilde{\mathcal{C}}_3\tilde{a}_s]\beta_0^2 - \tilde{a}_s\{p(1 + \tilde{\mathcal{C}}_1\tilde{a}_s + \tilde{\mathcal{C}}_2\tilde{a}_s^2 + \tilde{\mathcal{C}}_3\tilde{a}_s^3) + \tilde{a}_s[\tilde{\mathcal{C}}_1 + \tilde{a}_s(2\tilde{\mathcal{C}}_2 + 3\tilde{\mathcal{C}}_3\tilde{a}_s)]\}\beta_1\tilde{\beta}_2 \\ &+ \{p(1 + \tilde{\mathcal{C}}_1\tilde{a}_s + \tilde{\mathcal{C}}_2\tilde{a}_s^2 + \tilde{\mathcal{C}}_3\tilde{a}_s^3) + \tilde{a}_s[\tilde{\mathcal{C}}_1 + \tilde{a}_s(2\tilde{\mathcal{C}}_2 + 3\tilde{\mathcal{C}}_3\tilde{a}_s)]\}\beta_0(8\tilde{\beta}_2 + 3\tilde{a}_s\tilde{\beta}_3) = 0, \end{aligned} \tag{20}$$

$$\begin{aligned} &96\{(1+p)\tilde{\mathcal{C}}_1 + \tilde{a}_s[(2+p)\tilde{\mathcal{C}}_2 + (3+p)\tilde{\mathcal{C}}_3\tilde{a}_s]\}\beta_0^2 - 8\{p(1 + \tilde{\mathcal{C}}_1\tilde{a}_s + \tilde{\mathcal{C}}_2\tilde{a}_s^2 + \tilde{\mathcal{C}}_3\tilde{a}_s^3) + \tilde{a}_s[\tilde{\mathcal{C}}_1 + \tilde{a}_s(2\tilde{\mathcal{C}}_2 + 3\tilde{\mathcal{C}}_3\tilde{a}_s)]\}\beta_0\beta_1, \\ &+ \tilde{a}_s\{p(1 + \tilde{\mathcal{C}}_1\tilde{a}_s + \tilde{\mathcal{C}}_2\tilde{a}_s^2 + \tilde{\mathcal{C}}_3\tilde{a}_s^3) + \tilde{a}_s[\tilde{\mathcal{C}}_1 + \tilde{a}_s(2\tilde{\mathcal{C}}_2 + 3\tilde{\mathcal{C}}_3\tilde{a}_s)]\}\beta_1^2 = 0. \end{aligned} \tag{21}$$

Up to N^3-LO level, in addition to ρ_1, we need to determine two extra RG invariants ρ_2 and ρ_3, which can be fixed via a similar way as the NLO case; detailed procedures can be found in Refs. [13,20,47]. Then we obtain

$$\rho_2 = \mathcal{C}_2 - \frac{(1+p)\mathcal{C}_1^2}{2p} - \frac{\beta_1\mathcal{C}_1}{4\beta_0} + \frac{p\beta_2}{16\beta_0} \tag{22}$$

$$= \tilde{\mathcal{C}}_2 - \frac{(1+p)\tilde{\mathcal{C}}_1^2}{2p} - \frac{\beta_1\tilde{\mathcal{C}}_1}{4\beta_0} + \frac{p\tilde{\beta}_2}{16\beta_0} \tag{23}$$

and

$$\rho_3 = 2\mathcal{C}_3 + \frac{\mathcal{C}_1^2\beta_1}{4p\beta_0} - \frac{\mathcal{C}_1\beta_2}{8\beta_0} + \frac{p\beta_3}{64\beta_0} + \frac{2(1+p)(2+p)\mathcal{C}_1^3}{3p^2} - \frac{2(2+p)\mathcal{C}_1\mathcal{C}_2}{p} \tag{24}$$

$$= 2\tilde{\mathcal{C}}_3 + \frac{\tilde{\mathcal{C}}_1^2\beta_1}{4p\beta_0} - \frac{\tilde{\mathcal{C}}_1\tilde{\beta}_2}{8\beta_0} + \frac{p\tilde{\beta}_3}{64\beta_0} + \frac{2(1+p)(2+p)\tilde{\mathcal{C}}_1^3}{3p^2} - \frac{2(2+p)\tilde{\mathcal{C}}_1\tilde{\mathcal{C}}_2}{p}. \tag{25}$$

The first equations (22) and (24) are to set the value of $\rho_{2,3}$ with the known parameters calculated under the initial scheme and scale choices; the second equations (23) and (25) are due to scheme and scale independence of RG invariants $\rho_{2,3}$. As a cross check of those formulas, when setting $p = 1$, we turn to the same expressions as those of Ref. [13,20].

As a summary, in combination with all local RG equations, the known RG invariants, and also the same order int-β equation (9), we are ready to derive all the wanted optimal parameters. This can be done numerically by following the "spiraling" method [13,48,49]. For a general all-order determination, the procedures of the spiraling method are the following.

(i) First, one takes an initial value for $\tilde{a}_s$, which can be approximated by using an RG equation at the same order at an arbitrary initial scale. This initial scale should be large enough to ensure the pQCD calculation, which can be practically (to short the number of iterations) taken as the typical momentum flow of the process.

(ii) Second, for the first iteration, one sets the initial values for the scheme-dependent $\tilde{\beta}_2, \ldots, \tilde{\beta}_n$ to be $\beta_2, \ldots, \beta_n$ that have been calculated under an initial renormalization scheme. For new iterations their values are replaced by the ones determined from the last iteration. Then one solves the local RG equations, similar to Eqs. (13) and (17)–(21), for $\tilde{\mathcal{C}}_1, \ldots, \tilde{\mathcal{C}}_n$.

(iii) Third, one applies the calculated value of $\tilde{\mathcal{C}}_1, \ldots, \tilde{\mathcal{C}}_n$ into the equations on RG invariants $\rho_1, \ldots, \rho_n$, similar to Eqs. (12), (23), and (25), for $\tilde{a}_s, \tilde{\tau}, \tilde{\beta}_2, \ldots, \tilde{\beta}_n$.

(iv) Finally, one iterates from the second step until the results for ϱ_n converge to an acceptable prediction.

As a remarkable feature of renormalization theory, even if the coefficients $\mathcal{C}_n$ and the β terms β_n are separately different in different schemes, there exist some combinations of them that are RG invariant. The above derived integration parameters ρ_n are such kinds of RG invariants, which are key components to determine the "optimal ϱ_n." Because ρ_n are RG invariants, one can demonstrate that the final PMS predictions are independent of any choice of initial scale, being consistent with one of requirement of basic RG invariance [7]. Thus, to apply the PMS, one can simply set the initial scale to be a typical one such as the typical momentum of the process or the one at which the observable is measured. This, inversely, provides us a simpler/tricky way to derive the RG invariants ρ_n, which are put in the Appendix.

III. GENERAL PROPERTIES AND APPLICATIONS OF THE PMS SCALE SETTING

In this section, we shall present a detailed discussion on general properties of the PMS scale setting by utilizing three quantities $R_{e^+e^-}$, R_τ and $\Gamma(H \to b\bar{b})$ up to four-loop level. A comparison of the PMS and conventional scale settings shall also be presented.

A. $R_{e^+e^-}$ up to four-loop QCD corrections

The e^+e^- annihilation provides one of the most precise tests of pQCD theory. Its measurable quantity, i.e. the R ratio $R(Q)$, is defined as

$$R_{e^+e^-}(Q) = \frac{\sigma(e^+e^- \to \text{hadrons})}{\sigma(e^+e^- \to \mu^+\mu^-)} = 3\sum_q e_q^2[1 + R(Q)], \tag{26}$$

where Q stands for the e^+e^- collision energy at which the R ratio is measured. The pQCD approximant for $R(Q)$ up to $(n+1)$-loop correction can be written as

$$R_n(Q, \mu_0) = \sum_{i=0}^{n} \mathcal{C}_i(Q, \mu_0) a_s^{i+1}(\mu_0), \tag{27}$$

where μ_0 stands for an arbitrary initial scale and $a_s = \alpha_s/\pi$. Under the conventional scale setting, the renormalization scale shall be fixed to μ_0, while for a certain scale setting approach, the renormalization scale shall be varied from μ_0 to a certain degree.

The quantity $R_n(Q, \mu_0)$ has been calculated up to four-loop level under the $\overline{\text{MS}}$ scheme [21,22], whose coefficients for $\mu_0 = Q$ read

$$\mathcal{C}_0 = 1,$$
$$\mathcal{C}_1 = 1.9857 - 0.1152 n_f,$$
$$\mathcal{C}_2 = -6.63694 - 1.20013 n_f - 0.00518 n_f^2 - 1.240\eta,$$
$$\mathcal{C}_3 = -156.61 + 18.77 n_f - 0.7974 n_f^2 + 0.0215 n_f^3,$$

where $\eta = (\sum_q e_q)^2/(3\sum_q e_q^2)$, n_f and e_q stand for the number and electric charge of the active flavors. Because of the factorial growth of renormalon terms, the magnitude of the coefficient $\mathcal{C}_i$ generally grows with the increment of QCD loops, providing the dominant source for lessening the convergence of pQCD series. By applying the PMS, we shall show such a kind of factorial growth can be softened to a certain degree.

To do the numerical calculation, the QCD parameter $\Lambda_{\overline{\rm MS}}$ is fixed by using $\alpha_s(M_Z) = 0.1185 \pm 0.0006$ [50]. For self consistency, the $\Lambda_{\overline{\rm MS}}$ for R_n shall be determined by using $(n+1)_{\rm th}$-loop α_s-running determined from the RG equation (1). For example, we obtain $\Lambda_{\overline{\rm MS}}^{(n_f=5)} = 214$ MeV for R_3 by using four-loop α_s-running. Under the conventional scale setting, the renormalization scale shall be fixed to μ_0, while for the PMS, the renormalization scale shall be the optimal one determined from local RG invariance. In the following discussions, if not specially stated, we shall take $\mu_0 = Q$.

The coefficients $\mathcal{C}_1$, $\mathcal{C}_2$ and $\mathcal{C}_3$ before and after the PMS scale setting for various flavor numbers, i.e. $n_f = 3$, 4, and 5, are presented in Table I. Three typical scales, $Q = 1.2$, 3, and 31.6 GeV, are adopted for various flavor numbers. After applying the PMS, the magnitude of the coefficients $\mathcal{C}_i$ become smaller than those under the conventional scale setting, indicating that the divergent renormalon terms have been suppressed.

As for the conventional scale setting, one usually takes the same renormalization scale for pQCD predictions up to any perturbative order. Then, under the conventional scale setting, the effective coupling $\tilde{a}_s^{(n)} \equiv a_s^{(n)}$, and the slight differences among $\tilde{a}_s^{(n)}$ with various n are directly caused by the conventional α_s behavior up to $(n+1)$ loops. After applying the PMS, we shall have different effective/optimal coupling $\tilde{a}_s^{(n)}({\rm PMS})$ for each R_n. The effective coupling $\tilde{a}_s^{(n)}$ for R_n under those two scale settings is shown in Table II, where $n = 1$, 2, and 3, respectively. To determine the PMS effective coupling, one does not need to know the value of $\Lambda_{\rm QCD}$; thus the uncertainties from $\Lambda_{\rm QCD}$ are eliminated.[1] It is noted that the PMS effective coupling $\tilde{a}_s^{(n)}({\rm PMS})$ becomes smaller for a larger n, i.e. $\tilde{a}_s^{(1)}({\rm PMS}) > \tilde{a}_s^{(2)}({\rm PMS}) > \tilde{a}_s^{(3)}({\rm PMS})$. This agrees with the previous observation of Ref. [52] and is consistent with the "induced convergence" [53].

TABLE I. Coefficients for the perturbative expansion of $R_3(Q)$ before and after the PMS scale setting, where we have set $Q = 1.2$ GeV for $n_f = 3$, $Q = 3$ GeV for $n_f = 4$, and $Q = 31.6$ GeV for $n_f = 5$.

	$n_f = 3$	$n_f = 4$	$n_f = 5$
$\mathcal{C}_1$	1.6401	1.5249	1.4097
$\mathcal{C}_2$	−10.284	−11.6857	−12.8047
$\mathcal{C}_3$	−106.896	−92.9124	−80.0075
$\mathcal{C}_1^{\rm PMS}$	−0.458	−0.1105	0.0479
$\mathcal{C}_2^{\rm PMS}$	−1.1361	0.2103	1.3075
$\mathcal{C}_3^{\rm PMS}$	32.2133	24.9881	16.4108

TABLE II. The effective coupling $\tilde{a}_s^{(n)}$ under the conventional (Conv.) and the PMS scale settings, where $n = 1$, 2, and 3, respectively. Here we have set $Q = 1.2$ GeV for $n_f = 3$, $Q = 3$ GeV for $n_f = 4$, and $Q = 31.6$ GeV for $n_f = 5$.

	$n_f = 3$	$n_f = 4$	$n_f = 5$
$\tilde{a}_s^{(1)}({\rm Conv})$	0.1414	0.0823	0.0450
$\tilde{a}_s^{(2)}({\rm Conv})$	0.1320	0.0814	0.0450
$\tilde{a}_s^{(3)}({\rm Conv})$	0.1370	0.0820	0.0450
$\tilde{a}_s^{(1)}({\rm PMS})$	0.2156	0.1052	0.0504
$\tilde{a}_s^{(2)}({\rm PMS})$	0.1265	0.0832	0.0464
$\tilde{a}_s^{(3)}({\rm PMS})$	0.1212	0.0819	0.0461

TABLE III. The LO, NLO, N^{2}LO and N^{3}LO loop contributions for the approximant R_3 under the conventional and the PMS scale settings. The total column stands for the sum of all those loop corrections. $Q = 31.6$ GeV.

	LO	NLO	N^{2}LO	N^{3}LO	Total
Conv.	0.04499	0.00285	−0.00117	−0.00033	0.04635
PMS	0.04608	0.00010	0.00013	0.00007	0.04638

Next, we turn to numerical analysis of R_n under the PMS and conventional scale settings. For the purpose, we fix $Q = 31.6$ GeV, at which the R ratio has been measured [54].

Given a perturbative series, it is important to know how well it behaves, i.e., how much each loop term contributes. In Table III, we present the numerical results for the LO, NLO, N^{2}LO and N^{3}LO loop contributions to R_3 separately, in which the results for the conventional and the PMS scale settings are given. After applying the PMS, the magnitudes of the NLO, N^{2}LO and N^{3}LO loop terms become much smaller than the corresponding ones under the conventional scale setting. This is due to the combined effect of the suppression of renormalon terms and the induced convergence. However, this does not mean a more convergent pQCD series can be achieved. As shown by Table III, the pQCD series under the conventional scale setting has a standard perturbative convergence

$$|R_{3,{\rm Conv}}^{\rm LO}| \gg |R_{3,{\rm Conv}}^{\rm NLO}| > |R_{3,{\rm Conv}}^{\rm N^2LO}| > |R_{3,{\rm Conv}}^{\rm N^3LO}|,$$

[1]This property has been adopted for dealing with the coupling constant's fixed-point behavior at the low-energy region [14,15]. A detailed PMS analysis on physical observables at the low-energy region in comparison with those of the PMC and conventional scale settings is in preparation [51].

which is mainly caused by α_s-power suppression. On the other hand, the PMS prediction shows a quite different perturbation series, i.e.,

$$R^{\rm LO}_{3,\rm PMS} \gg R^{\rm NLO}_{3,\rm PMS} \sim R^{\rm N^2LO}_{3,\rm PMS} \sim R^{\rm N^3LO}_{3,\rm PMS}$$

with $R^{\rm N^2LO}_{3,\rm PMS} > R^{\rm NLO}_{3,\rm PMS}$. The PMS prediction is determined by local RG invariance; thus its goal is to achieve the steady behavior of a perturbative series rather than to improve its pQCD convergence. For example, the LO term $R^{\rm LO}_{3,\rm PMS}$ provides over 99% of contributions to the PMS series, and the PMS prediction quickly approaches its steady behavior. However, its pQCD convergence can only be an accidental or it shall not show pQCD convergence at all.

To show to what degree a low-order prediction can be improved by a high-order one, we define a ratio

$$\kappa_n = \frac{R_n - R_{n-1}}{R_{n-1}}. \qquad n = (1,2,3).$$

To be a "convergent and accurate" $(n+1)$-loop pQCD prediction, one would think that the magnitude of κ_n should be small enough and also be smaller than $\kappa_{(n-1)}$. Numerical results for R_n and κ_n up to four-loop level before and after the PMS scale setting are presented in Table IV. It shows that both conventional and PMS scale settings can give acceptable predictions when more high-order corrections have been taken into consideration. Up to four-loop level, the absolute values of κ_3 for the conventional and PMS scale settings are smaller than 1%, indicating that the pQCD predictions for this case are convergent and accurate enough, i.e., the four-loop prediction R_3 is very close to the true value of the physical observable R. Following the trends of those predictions, we can expect that the physical value of R could be around 0.04635.

Previously, there was a doubt casted on the usefulness of the PMS [19] because it gives larger κ_1 and κ_2 than the conventional scale setting does. However the absolute value of the PMS κ_3 is smaller than its counterpart of the conventional scale setting by about three times. This indicates that a larger PMS κ_1 and κ_2 only reflect the importance of N^3-LO correction for the PMS to achieving a better prediction than the conventional scale setting. Thus the available N^3-LO correction helps us to clarify such kinds of doubts on the PMS.

TABLE IV. Numerical results for R_n and κ_n with various QCD loop corrections under the conventional and PMS scale settings. The value of $R_0 = 0.04454$ is the same for both scale settings. $Q = 31.6$ GeV.

	R_1	R_2	R_3	κ_1	κ_2	κ_3
Conv.	0.04786	0.04666	0.04635	7.44%	−2.50%	−0.66%
PMS	0.04889	0.04644	0.04638	9.76%	−5.00%	−0.14%

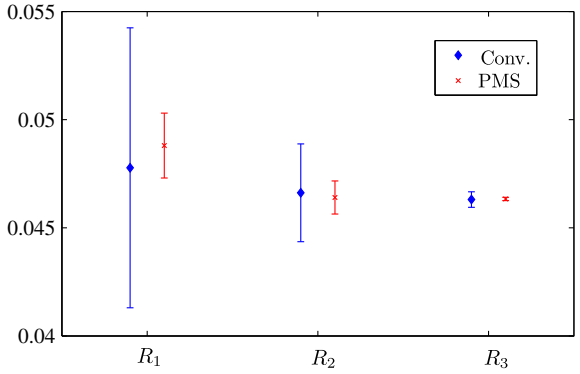

FIG. 1 (color online). Results for R_n $(n = 1, 2, 3)$ together with their error estimates $(\pm|\tilde{\mathcal{C}}_n \tilde{a}_s^{n+1}|_{\rm MAX})$. The diamonds and the crosses are for conventional and PMS scale settings, respectively. $Q = 31.6$ GeV.

It is helpful to find a way to predict unknown high-order pQCD corrections. Conventionally, this is done by varying the renormalization scale over a certain range, e.g. $\mu_0 \in [Q/2, 2Q]$. This conventional error estimate is not reliable, since it only partly estimates the high-order non-conformal contribution but not the more important conformal one [7]. It is no reason to choose $1/2$ or 2 to discuss the error; why not three times or others? Moreover, for a scale setting such as PMS or PMC, it is unreasonable to simply vary their optimal scales via a similar way to predict unknown high-order pQCD corrections, since this way breaks the RG invariance and leads to unreliable results. As a conservative prediction, one can take the perturbative uncertainty to be one of the last known order [13], i.e. the unknown high-order pQCD correction is taken as $(\pm|\mathcal{C}_n \tilde{a}_s^{n+1}|_{\rm MAX})$ for a $(n+1)$-loop prediction of R_n, where $|\mathcal{C}_n a_s^{n+1}|$ is calculated by varying $\mu_0 \in [Q/2, 2Q]$[2] and the symbol "MAX" stands for the maximum $|\mathcal{C}_n a_s^{n+1}|$ within this scale region. The error estimates for conventional and PMS scale settings are displayed in Fig. (1). It shows that the PMS errors are smaller than those under the conventional scale setting, which tend to shrink more rapidly with the increment of pQCD order. It is noted that the PMS R_2 and R_3 lie well outside the error estimation of R_1. Thus the PMS prediction on R_1 alone is not able to predict correct high-order contributions. Such an improper PMS prediction on R_1 also explains why the PMS κ_1 and κ_2 are so large. However by including more high-order contributions, the PMS works better and gives more reliable predictions.

Finally, we discuss the scale dependence of R_n under different scale settings. We present the scale dependence of $R_n^{\rm Conv}(31.6\ {\rm GeV}, \mu_0)$ up to four-loop level under the conventional scale setting in Fig. (2). The LO and NLO estimations, R_0 and R_1, depend heavily on μ_0. When more high-order

[2]As shown by the latter Fig. (3) the PMS prediction is independent to the choice of μ_0; thus such choice of the usual scale range only leads to a smaller conventional scale error.

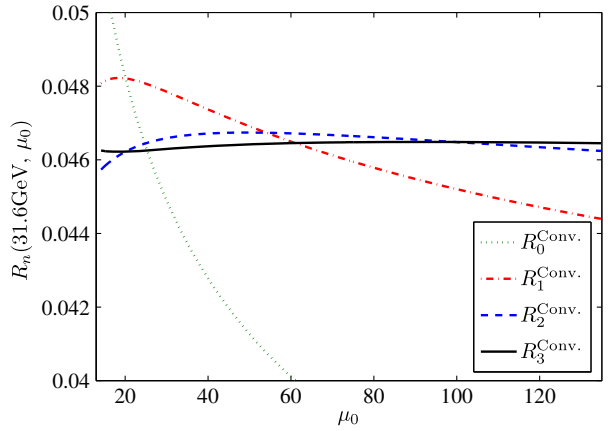

FIG. 2 (color online). The pQCD prediction $R_n^{\text{Conv}}(Q = 31.6\ \text{GeV}, \mu_0)$ up to four-loop level versus the initial scale μ_0. The dotted, the dash-dot, the dashed and the solid lines are for R_0, R_1, R_2 and R_3, respectively.

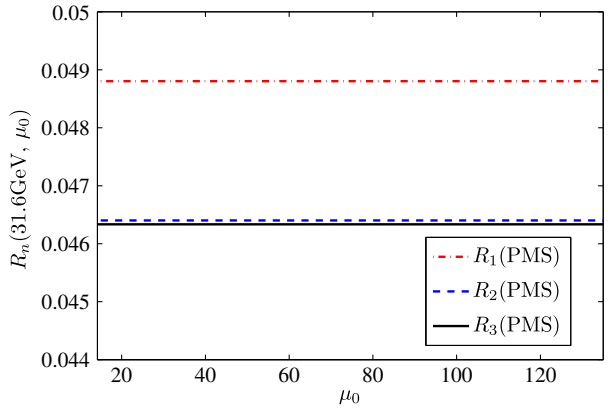

FIG. 3 (color online). The pQCD prediction $R_n^{\text{PMS}}(Q = 31.6\ \text{GeV}, \mu_0)$ up to four-loop level versus the initial scale μ_0. The dash-dot, the dashed and the solid lines are for, R_1, R_2 and R_3, respectively.

corrections have been taken into account, the scale dependence becomes weaker. This agrees with the conventional wisdom that, by computing high-order enough corrections, one may get scale-independent predictions. However, not all quantities in pQCD can be calculated to accurate enough high orders due to the complexity of high-loop QCD calculations. As a comparison, we present the scale dependence of $R_n^{\text{PMS}}(31.6)$ GeV under the PMS scale setting in Fig. (3). It shows that the PMS does eliminate the initial scale dependence even for low fixed-order pQCD predictions, which is consistent with our previous conclusions drawn from the properties of RG invariants.

B. R_τ up to four-loop level

The ratio for τ-lepton decays into hadrons is defined as

$$R_\tau = \frac{\Gamma(\tau \to \nu_\tau + \text{hadrons})}{\Gamma(\tau \to \nu_\tau + e^- \bar{\nu}_e)}, \tag{28}$$

which provides another fundamental test of pQCD and it can be calculated from $R_{e^+e^-}$ [55,56]:

$$R_\tau(M_\tau) = 2\int_0^{M_\tau^2} \frac{ds}{M_\tau^2}\left(1 - \frac{s}{M_\tau^2}\right)^2\left(1 + \frac{2s}{M_\tau^2}\right)\tilde{R}_{e^+e^-}(\sqrt{s}).$$

Here $M_\tau = 1.777$ GeV [50] is the τ-lepton mass, s stands for the squared invariant mass of hadrons, and $\tilde{R}_{e^+e^-}(\sqrt{s})$ can be obtained from $R_{e^+e^-}$ by replacing $3\sum_q e_q^2$ with $3(|V_{ud}|^2 + |V_{us}|^2) \approx 3$.

After doing the integration over s and putting the explicit scale dependence into the expression, we can rewrite R_τ as

$$R_\tau(M_\tau, \mu_0) = 3(|V_{ud}|^2 + |V_{us}|^2)(1 + r_n^\tau(M_\tau, \mu_0)), \tag{29}$$

where the perturbative approximant

$$r_n^\tau(M_\tau, \mu_0) = \sum_{i=0}^{n} C_i'(M_\tau, \mu_0) a_s^{i+1}(\mu_0). \tag{30}$$

μ_0 stands for initial renormalization scale. At $\mu_0 = M_\tau$, the coefficients of R_τ under the $\overline{\text{MS}}$ scheme up to four-loop level can be written as [21]

$$\begin{aligned} C_0' &= 1, \\ C_1' &= 6.3399 - 0.3791 n_f, \\ C_2' &= 48.5831 - 7.87865 n_f + 0.15786 n_f^2, \\ C_2' &= 401.54 - 109.449 n_f + 6.18148 n_f^2 - 0.06366 n_f^3. \end{aligned}$$

We start from the (initial) scale dependence of $r_n^\tau(M_\tau)$. The results for r_n^τ under the conventional scale setting are put in Fig. (4). It is found that the approximant r_n^τ strongly depends on μ_0 even for the four-loop prediction. This indicates that we need even more loop terms to make the final prediction accurate enough. On the other hand, after

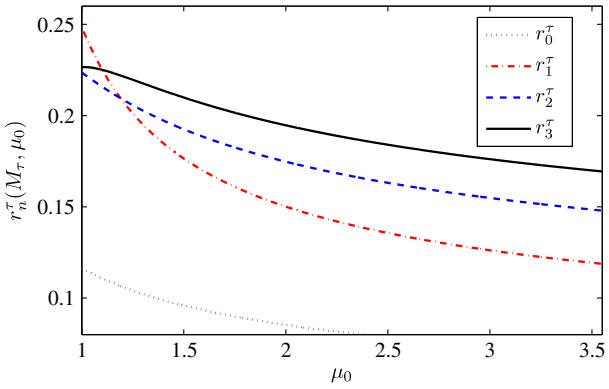

FIG. 4 (color online). The pQCD prediction $r_n^\tau(M_\tau, \mu_0)$ up to four-loop level versus the initial scale μ_0 under the conventional scale setting. The dotted, the dash-dot, the dashed and the solid lines are for r_0^τ, r_1^τ, r_2^τ and r_3^τ, respectively.

TABLE V. Coefficients for the perturbative expansion of r_3^τ before and after the PMS scale setting. $\mu_0 = M_\tau$.

	$\mathcal{C}'_1$	$\mathcal{C}'_2$	$\mathcal{C}'_3$
Conv.	5.2023	26.3659	127.079
PMS	0.3906	1.2380	−6.1747

TABLE VI. The effective couplings $\tilde{a}_s^{(n)}$ for r_n^τ under the conventional and PMS scale settings. $\mu_0 = M_\tau$.

	$\tilde{a}_s^{(1)}$	$\tilde{a}_s^{(2)}$	$\tilde{a}_s^{(3)}$
Conv.	0.1042	0.1015	0.1032
PMS	0.4733	0.1963	0.1994

TABLE VII. The LO, NLO, N^{2}LO and N^{3}LO loop contributions for the approximant r_3^τ under the conventional and the PMS scale settings. The total column stands for the sum of all those loop corrections.

	LO	NLO	N^{2}LO	N^{3}LO	Total
Conv.	0.10320	0.05541	0.02898	0.01441	0.20200
PMS	0.19935	0.01552	0.00981	−0.00975	0.21493

applying the PMS, we get the same initial scale independence at any orders as that of Fig. (3). In the following, we shall take $\mu_0 = M_\tau$ to do our discussions.

The coefficients $\mathcal{C}'_n$ before and after the PMS scale setting are presented in Table V. Again the factorial renormalon growth of $\mathcal{C}'_n$ has been suppressed. The effective couplings $\tilde{a}_s^{(n)}$ for r_n^τ under the conventional and PMS scale settings are presented in Table VI. Unlike the case of R_n, there is no induced convergence for r_n^τ, i.e. $\tilde{a}_s^{(1)} > \tilde{a}_s^{(2)} \sim \tilde{a}_s^{(3)}$. Thus the induced convergence can only be an approximate property of the PMS.

In Table VII, we present numerical results for the LO, NLO, N^{2}LO and N^{3}LO loop contributions to r_3^τ separately, in which the results for conventional and PMS scale settings are presented. The magnitude of the N^3-LO term under the conventional scale is about 7% of r_3^τ, which changes down to ∼4% after applying the PMS scale setting. The pQCD series under the conventional scale setting shows a standard perturbative convergence similar to the case of R_n. And the PMS prediction also shows a different perturbation series, i.e.,

$$r_{3,\mathrm{PMS}}^{\tau,\mathrm{LO}} \gg r_{3,\mathrm{PMS}}^{\tau,\mathrm{NLO}} > r_{3,\mathrm{PMS}}^{\tau,\mathrm{N^2LO}} \sim |r_{3,\mathrm{PMS}}^{\tau,\mathrm{N^3LO}}|.$$

Numerical results for r_n^τ and κ_n^τ under conventional and PMS scale settings are presented in Table VIII. The value of κ_3^τ under both scale settings is around 10%, indicating the necessity of calculating more high-order terms before an accurate pQCD prediction on R_τ can be achieved. $\kappa_3^\tau(\mathrm{PMS})$ is slightly smaller than $\kappa_3^\tau(\mathrm{Conv})$; thus the PMS can lead to relatively better four-loop prediction than the conventional scale setting. The PMS r_1^τ is about 2.2 times larger than the conventional one, which provides the reason for large κ_1^τ and κ_2^τ.

TABLE VIII. Numerical results for r_n^τ and κ_n^τ with various QCD loop corrections under the conventional and PMS scale settings. The value of $r_0^\tau = 0.0897$ is the same for both scale settings. $\mu_0 = M_\tau$.

	r_1^τ	r_2^τ	r_3^τ	κ_1^τ	κ_2^τ	κ_3^τ
Conv.	0.16064	0.18255	0.20200	79.18%	13.64%	10.66%
PMS	0.36514	0.19781	0.21493	307.29%	−45.83%	8.66%

Results for r_n^τ $(n = 1, 2, 3)$ together with their error estimates, i.e. the predicted unknown high-order contributions $(\pm|\tilde{\mathcal{C}}'_n \tilde{a}_s^{n+1}|_{\mathrm{MAX}})$, are presented in Fig. (5). Similar to the $R_{e^+e^-}$ case, $r_{2,3}^\tau$ are outside the prediction of r_1^τ. The PMS r_1^τ is even outside the conventional prediction of r_1^τ with large errors. Thus, the PMS prediction on r_1^τ alone is not able to predict correct high-order contributions. But the PMS provides smaller errors for r_2^τ and r_3^τ than those given by the conventional method, and the PMS errors shrink quickly when more loop corrections are included. Using the four-loop prediction, we obtain

$$R_\tau(M, \mu_0)|_{\mathrm{Conv}} = 3.606 \pm 0.111, \tag{31}$$

$$R_\tau(M, \mu_0)|_{\mathrm{PMS}} = 3.645 \pm 0.029, \tag{32}$$

where the errors are predicted high-order contributions for $\mu_0 \in [M/2, 2M]$. Both of them are consistent with the OPAL measurement [57], $R_\tau = 3.593 \pm 0.008$. These values strongly depend on the choice of $\Lambda_{\mathrm{QCD}}^{n_f=3}$. Inversely, by

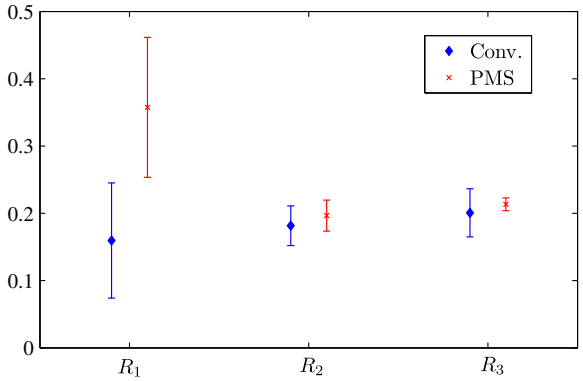

FIG. 5 (color online). Results for r_n^τ $(n = 1, 2, 3)$ together with their errors $(\pm|\tilde{\mathcal{C}}'_n \tilde{a}_s^{n+1}|_{\mathrm{MAX}})$. The diamonds and the crosses are for the conventional scale setting and the PMS.

using the OPAL data on R_τ and following the approach suggested in Ref. [13], we predict $\Lambda^{n_f=3}_{\rm Conv} = 340^{+4}_{-5}$ MeV and $\Lambda^{n_f=3}_{\rm PMS} = 323^{+4}_{-4}$ MeV.

C. $\Gamma(H \to b\bar{b})$ up to four-loop level

The decay width for Higgs bosons decaying into a $b\bar{b}$ pair can be written as

$$\Gamma(H \to b\bar{b}) = \frac{3G_F M_H m_b^2(M_H)}{4\sqrt{2}\pi}(1+\tilde{R}_n), \qquad (33)$$

where G_F is the Fermi constant, M_H is the mass of the Higgs boson, and $m_b(M_H)$ is the b-quark $\overline{\rm MS}$ running mass, and up to $(n+1)$-loop level, we have

$$\tilde{R}_n(M_H,\mu_0) = \sum_{i=0}^{n} \tilde{C}_i''(M_H,\mu_0) a_s^{i+1}(\mu_0),$$

where μ_0 stands for an arbitrary initial scale. The QCD corrections for the decay width $\Gamma(H \to b\bar{b})$ have been calculated up to four-loop level, cf. Refs. [23,24,58,59]; for $\mu_0 = M_H$, the four-loop $\tilde{R}_3$ reads [23]

$$\begin{aligned}\tilde{R}_3 = {} & 5.6667 a_s(M_H) + (35.94 - 1.359 n_f) a_s^2(M_H) + (164.14 - 25.77 n_f + 0.259 n_f^2) a_s^3(M_H) \\ & + (39.34 - 220.9 n_f + 9.685 n_f^2 - 0.0205 n_f^3) a_s^4(M_H). \end{aligned} \qquad (34)$$

The initial scale dependence of $\tilde{R}_n$ under the conventional scale setting is presented in Fig. (6). The scale dependence becomes weaker with the increment of high-loop terms, and the four-loop prediction $\tilde{R}_3$ is almost independent to the scale changes. This is the standard properties of pQCD prediction from the conventional scale setting, which however cannot weaken the importance of a more proper scale setting. For example, after applying the PMS, we get the same initial scale independence at lower orders as that of Fig. (3).

The coefficients C_n'' before and after the PMS scale setting in Table IX. Because of the renormalon term, the absolute value of $C_3'' \sim 826$, which changes down to $\sim$143 by applying the PMS. The effective couplings $\tilde{a}_s^{(n)}$ for $\tilde{R}_n$ under conventional and PMS scale settings are presented in Table X. For the present case, the effective couplings $\tilde{a}_s$ for the conventional scale setting are almost unchanged, while the PMS ones decreases with the increment of loop terms.

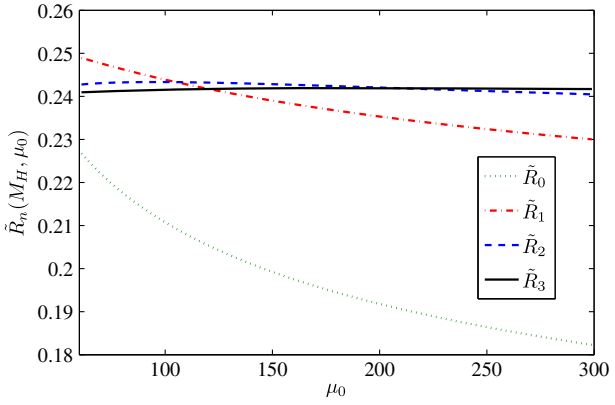

FIG. 6 (color online). The pQCD prediction $\tilde{R}_n(M_H,\mu_0)$ up to four-loop level versus the initial scale μ_0 under the conventional scale setting. The dotted, the dash-dot, the dashed and the solid lines are for $\tilde{R}_0$, $\tilde{R}_1$, $\tilde{R}_2$, and $\tilde{R}_3$, respectively.

The LO, NLO, N^{2}LO and N^{3}LO loop contributions for the approximant $\tilde{R}_3$ under conventional and PMS scale settings are presented in Table XI. The LO term provides dominant contribution to $\tilde{R}_3$. The magnitude of the N^3-LO term under the conventional scale setting provides a smaller $\sim$0.6% contribution to $\tilde{R}_3$, which changes down to 0.2% after applying the PMS scale setting. The pQCD series under the conventional scale setting shows a standard perturbative convergence similar to the case of R_n. And

TABLE IX. Coefficients for the perturbative expansion of $\tilde{R}_3$ before and after the PMS scale setting. $\mu_0 = M_H$.

	C_1''	C_2''	C_3''
Conv.	29.145	41.765	−825.598
PMS	0.34376	21.2286	−142.849

TABLE X. The effective couplings $\tilde{a}_s^{(n)}$ for $\tilde{R}_n$ under the conventional and PMS scale settings. $\mu_0 = M_H$.

	$\tilde{a}_s^{(1)}$	$\tilde{a}_s^{(2)}$	$\tilde{a}_s^{(3)}$
Conv.	0.0360	0.0360	0.0359
PMS	0.0465	0.0425	0.0423

TABLE XI. The LO, NLO, N^{2}LO and N^{3}LO loop contributions for the approximant $\tilde{R}_3$ under the conventional and the PMS scale settings. The total column stands for the sum of all those loop corrections. $\mu_0 = M_H$.

	LO	NLO	N^{2}LO	N^{3}LO	Total
Conv.	0.20371	0.03767	0.00194	−0.00138	0.24194
PMS	0.23967	0.00061	0.00161	−0.00046	0.24144

TABLE XII. Numerical results for $\tilde{R}_n$ and $\tilde{\kappa}_n$ with various QCD loop corrections under the conventional and PMS scale settings. The value of $\tilde{R}_0 = 0.20419$ is the same for both scale settings. $\mu_0 = M_H$.

	$\tilde{R}_1$	$\tilde{R}_2$	$\tilde{R}_3$	$\tilde{\kappa}_1$	$\tilde{\kappa}_2$	$\tilde{\kappa}_3$
Conv.	0.24151	0.24333	0.24194	18.28%	0.75%	−0.57%
PMS	0.25621	0.24087	0.24144	25.48%	−5.99%	0.24%

the PMS prediction also shows a different perturbation series, i.e.,

$$\tilde{R}^{\rm LO}_{3,\rm PMS} \gg \tilde{R}^{\rm NLO}_{3,\rm PMS}, \tilde{R}^{\rm N^2LO}_{3,\rm PMS}, \tilde{R}^{\rm N^3LO}_{3,\rm PMS}$$

with $\tilde{R}^{\rm N^2LO}_{3,\rm PMS} > \tilde{R}^{\rm NLO}_{3,\rm PMS}$.

Numerical results for $\tilde{R}_n$ and $\tilde{\kappa}_n$ up to four-loop level are presented in Table XII. Results for $\tilde{R}_n$ $(n = 1, 2, 3)$ together with their prediction of unknown high-order contributions $(\pm|\tilde{C}''_n \tilde{a}_s^{n+1}|_{\rm MAX})$ are presented in Fig. (7). The four-loop $\tilde{R}_3$ are nearly the same for conventional and PMS scale settings, while the PMS $\tilde{\kappa}_3$ is smaller and more close to its final prediction on the observable $\tilde{R}$. However, the PMS $\tilde{R}_1$ also cannot predict the correct high-order contributions, i.e. both $\tilde{R}_2$ and $\tilde{R}_3$ are outside its prediction. Such a larger PMS $\tilde{R}_1$ also leads to larger $\tilde{\kappa}_1$ and $\tilde{\kappa}_2$. With those $\tilde{R}_3$ results, we present the decay width of a Higgs boson into a $b\bar{b}$ pair:

$$\Gamma(H \to b\bar{b})|_{\rm Conv} = 2389.85 \pm 3.85 \text{ KeV}, \quad (35)$$

$$\Gamma(H \to b\bar{b})|_{\rm PMS} = 2388.87 \pm 0.88 \text{ KeV}, \quad (36)$$

where the errors are predicted unknown high-order contributions for $\mu_0 \in [M_H/2, 2M_H]$.

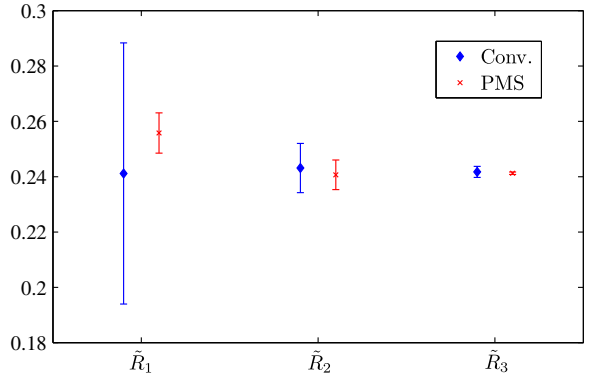

FIG. 7 (color online). Results for $\tilde{R}_n$ $(n = 1, 2, 3)$ together with their prediction of unknown high-order contributions $(\pm|\tilde{C}''_n \tilde{a}_s^{n+1}|_{\rm MAX})$ for $H \to b\bar{b}$. The diamonds and the crosses are for conventional and PMS scale settings, respectively.

TABLE XIII. Coefficients $C_n^{\rm PMC}$ for the perturbative expansion of $R_3(Q)$ using the PMC scale setting, where we have set $Q = 1.2$ GeV for $n_f = 3$, $Q = 3$ GeV for $n_f = 4$, and $Q = 31.6$ GeV for $n_f = 5$.

	$n_f = 3$	$n_f = 4$	$n_f = 5$
$C_1^{\rm PMC}$	2.14579	1.99302	1.84024
$C_2^{\rm PMC}$	3.39697	1.21574	−1.00503
$C_3^{\rm PMC}$	6.47103	−12.8517	−11.0871

TABLE XIV. A comparison of R_n and κ_n under the PMS and PMC scale settings. The value of $R_0 = 0.04454$ is the same for both scale settings. $Q = 31.6$ GeV and $\mu_0 = Q$.

	R_1	R_2	R_3	κ_1	κ_2	κ_3
PMS	0.04889	0.04644	0.04638	9.76%	−5.00%	−0.14%
PMC	0.04767	0.04667	0.04635	7.03%	−2.09%	−0.69%

IV. A COMPARISON OF THE PMS AND PMC

The running behavior of the coupling constant is controlled by the RG equation. Unlike the local RG invariance of the PMS, the PMC [26–32] respects the standard RG invariance and improves the perturbative series by absorbing all β-terms governed by the RG equation into the coupling constant. The PMC procedure can be advantageously applied to an entire range of perturbatively calculable QCD and standard model processes. Recently, many high-order PMC applications have been finished and the PMC works successfully, cf. Refs. [60–64]. It is helpful to present a detailed comparison of PMS and PMC predictions. For the purpose, we take $R_{e^+e^-}$ as an explicit example.

After applying the PMC, the coefficients $C_n^{\rm PMC}$ for R_3 are presented in Table XIII. Comparing with Table I, PMC coefficients are smaller than the conventional ones. The PMS also leads to such a suppression, but it cannot explain why. The PMC shows that such suppressions are rightly due to the elimination of renormalon terms.

A comparison of R_n and κ_n under PMS and PMC scale settings is presented in Table XIV. The differences for

TABLE XV. The LO, NLO, N^{2}LO and N^{3}LO loop contributions for the approximant R_3 under the PMS and PMC scale settings. The total column stands for the sum of all those loop corrections. $Q = 31.6$ GeV and $\mu_0 = Q$.

	LO	NLO	N^{2}LO	N^{3}LO	Total
PMS	0.04608	0.00010	0.00013	0.00007	0.04638
PMC	0.04290	0.00351	−0.00004	−0.00002	0.04635

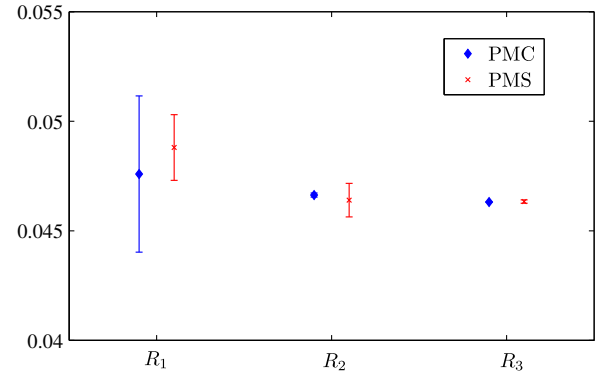

FIG. 8 (color online). A comparison of PMC and PMS predictions for R_n $(n = 1, 2, 3)$ together with their predicted unknown high-order contributions $(\pm|\tilde{\mathcal{C}}_n \tilde{a}_s^{n+1}|_{\rm MAX})$. The diamonds and the crosses are for PMC and PMS scale settings, respectively.

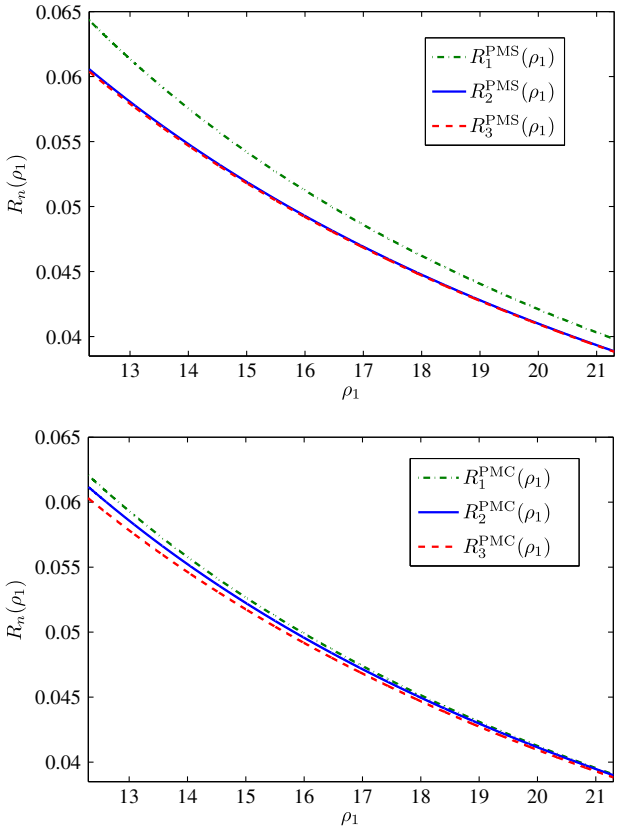

FIG. 9 (color online). The curves of the function $R_n(\rho_1)$ for the PMS and PMC scale settings. $\mu_0 = Q$.

three-loop R_2 are about 0.5%, which moves down to about 0.05% for four-loop R_3. Both the PMS and PMC are based on RG invariance; it is reasonable that they can give close numerical predictions at higher orders. The values of the PMC κ_1 and κ_2 are smaller than those of the PMS, indicating that a faster steady behavior can be achieved by the PMC.[3]

TABLE XVI. The difference δ_n for $R_n(\rho 1)$ between the PMC (or conventional) scale setting and the PMS scale setting.

	δ_1	δ_2	δ_3
Conv.	2.24%	0.55%	0.10%
PMC	2.66%	0.61%	0.07%

A comparison of PMS and PMC pQCD series is presented in Table XV. The PMC pQCD series follows the standard pQCD convergence but is much more convergent than that of the conventional scale setting, while the PMS series also becomes more convergent than the conventional ones, but the series does not show the order-by-order convergence, i.e. $R^{\rm N^2LO}_{3,\rm PMS} > R^{\rm NLO}_{3,\rm PMS}$.

In Fig. (8), we present a comparison of PMC and PMS predictions for R_n $(n = 1, 2, 3)$ together with their predicted unknown high-order contributions $(\pm|\tilde{\mathcal{C}}_n \tilde{a}_s^{n+1}|_{\rm MAX})$. The large error bar for the PMC R_1 shows that the magnitude of the NLO-conformal terms are large and we need even high-order terms to achieve an accurate prediction. In fact, when we have more β-terms to fix the PMC scales, the PMC prediction together with its predicted error does become more accurate.

We present a comparison of the PMS and PMC energy dependence of $R_n(Q)$ in Fig. (9), where we have changed the argument to ρ_1 such as to avoid the uncertainty from $\Lambda_{\rm QCD}$ [20]. The present range $\rho_1 \in (12, 21)$ corresponds to energy range $9 < Q < 90$ GeV. There is a large difference between $R_1^{\rm PMS}(\rho_1)$ and $R_{n\geq 2}^{\rm PMS}(\rho_1)$, which is consistent with a previous observation that $R_1^{\rm PMS}(\rho_1)$ alone cannot predict reasonable unknown high-order contributions. To show the difference of the predicted $R_n(\rho_1)$ under various scale settings more accurately, we define a parameter, δ_n, as

$$\delta_n = \frac{\sum_{\rho_1} |R_n(\rho_1) - R_n^{\rm PMS}(\rho_1)|}{\sum_{\rho_1} |R_n^{\rm PMS}(\rho_1)|} \times 100\%, \qquad (37)$$

where $\rho_1 = 12, 12.001, 12.002, \ldots, 21$. Those differences are presented in Table XVI. The differences of $R_n(\rho_1)$ among different scale settings shall be reduced with more loop corrections being included.

V. SUMMARY

To solve the renormalization scheme and renormalization scale ambiguities, one should answer the question of how to set optimal scale systematically for any physical processes up to any orders from some basic principle of

[3]The PMS κ_3 for $R_{e^+e^-}$ is accidentally small. We have found that the PMC κ_3 for R_τ and $\Gamma(H \to b\bar{b})$ are smaller than those of the PMS, following the same trends.

QCD theory. As a practical solution, the PMS adopts local RG invariance (7)–(8) to set the optimal scheme and optimal scale of the process.

Based on the local RG invariance, we have presented the detailed technology for applying the PMS to high-perturbative orders. We have investigated the PMS properties based on three typical physical quantities $R_{e^+e^-}$, R_τ and $\Gamma(H \to b\bar{b})$ up to four-loop QCD corrections. Our analysis show that even though the PMS is theoretically unsound, it does provide an effective approach to soften the renormalization scheme and scale ambiguities by including enough higher-order pQCD contributions. More explicitly, our results show the following.

(i) After applying the PMS, the magnitudes of perturbative coefficients become smaller than those under the conventional scale setting, indicting that the divergent renormalon terms can be suppressed. The PMS effective coupling approximately satisfies the induced convergence. As a combined effect, the magnitudes of NLO and higher-order loop terms become much smaller than the corresponding ones under the conventional scale setting.

(ii) The goal of the PMS is to achieve the steady point of a perturbative series over the renormalization scheme and scale changes. The PMS predictions for those three four-loop examples do show such a steady behavior, i.e. the final PMS predictions are independent of any choice of initial scale, being consistent with one of the requirements of basic RG invariance. Moreover, the LO terms $R^{\rm LO}_{3,\rm PMS}$ and $\tilde{R}^{\rm LO}_{3,\rm PMS}$ provide ∼99% contributions, and $r_3^{\tau,\rm LO}$ provides ∼89% contribution to $R_{e^+e^-}$, $\Gamma(H \to b\bar{b})$ and R_τ series, respectively. However, the PMS has no principle to ensure the pQCD convergence; thus the improved pQCD convergence for some of the high-energy processes could only be an accidental. In fact, all those three four-loop examples do not have standard pQCD convergence, i.e. the magnitudes of their NLO, N^{2}LO and N^{3}LO terms are usually small but at the same order.

(iii) We have suggested a conservative way to discuss the pQCD predictive power, i.e. to show how unknown high-order terms contribute. It is noted that after the PMS scale setting, the N^{2}LO and N^{3}LO estimates are usually outside the predicted errors by using the terms only up to NLO level. Together with other lower-order PMS behaviors, such as the large PMS $\kappa_{1,2}$ for the mentioned processes, we may conclude that the PMS cannot provide correct lower-order predictions, such as the NLO predictions. In the literature, most of the doubts on the PMS are rightly based on lower-order predictions. With more loop corrections being included, the PMS can achieve a more accurate prediction than that of conventional scale setting.

In this paper, we have also presented a comparison of PMS and PMC predictions. Unlike the PMS, the PMC satisfies standard RG invariance and follows the RG equation to fix the running behavior of the coupling constant; thus it is theoretically sound. The PMC predictions have optimal pQCD convergence due to the elimination of renormalon terms. The PMS prediction is independent on the choice of initial scale, while there is residual scale dependence for PMC predictions due to unknown high-order β-term; however such residual scale dependence is highly suppressed, even for lower-order PMC predictions. In comparison to the conventional and PMS scale settings, the PMC shows a better predictive power, and its predictions quickly approach the physical value of the observable. Moving to high-order pQCD predictions, the PMS and PMC differences on the pQCD predictions shall be greatly suppressed, e.g. for the case of $R_{e^+e^-}$, the differences change from larger ∼3% at the NLO level, to ∼1% at the N^{2}LO level, to less than 0.1% at the N^3-LO level.

ACKNOWLEDGMENTS

We thank Stanley J. Brodsky, Hai-Bing Fu, Matin Mojaza, Paul M. Stevenson, Sheng-Quan Wang, and Xu-Chang Zheng for helpful discussions. This work was supported in part by Natural Science Foundation of China under Grant No. 11275280 and by the Fundamental Research Funds for the Central Universities under Grant No. CQDXWL-2012-Z002.

APPENDIX A: A TRICKY WAY TO DERIVE THE RG INVARIANTS ρ_n AT HIGH ORDERS

In this Appendix, we present a simpler way to derive the RG invariants ρ_n at high orders with $n > 1$, based on their properties of RG invariance.

For convenience, we set $p = 1$ in Eq. (3) and redefine the $\beta^{\mathcal{R}}$-function as

$$\beta^{\mathcal{R}} = \mu^2 \frac{\partial}{\partial \mu^2}\left(\frac{\alpha_s(\mu)}{4\pi}\right) = -\sum_{i=0}^{\infty} b_i a_s^{i+2}, \qquad \text{(A1)}$$

where $b_i = (1/4)^{i+2}\beta_i^{\mathcal{R}}$ and $a_s = \alpha_s/\pi$.

A physical observable solitarily defines an effective charge [65,66], and vice versa. Thus, we can inversely write down the coupling constant a_s as an expression over the approximant ϱ_n [67], i.e.

$$a_s(\varrho_n) = \varrho_n + \sum_{i=1}^{\infty} r_i {\varrho_n}^{i+1}. \qquad \text{(A2)}$$

Substituting the ϱ_n expression (3) into Eq. (A2), we obtain

$$a_s = a_s(1 + \mathcal{C}_1 a_s + \mathcal{C}_2 a_s^2 + \mathcal{C}_3 a_s^3 + \cdots)[1 + r_1 a_s(1 + \mathcal{C}_1 a_s + \mathcal{C}_2 a_s^2 + \mathcal{C}_3 a_s^3 + \cdots) + r_2 a_s^2(1 + \mathcal{C}_1 a_s + \mathcal{C}_2 a_s^2 + \mathcal{C}_3 a_s^3 + \cdots)^2 + \cdots] \tag{A3}$$

$$= a_s[1 + a_s(r_1 + \mathcal{C}_1) + a_s^2(2r_1\mathcal{C}_1 + r_2 + \mathcal{C}_2) + a_s^3(r_1\mathcal{C}_1^2 + 2r_1\mathcal{C}_2 + 3r_2\mathcal{C}_1 + r_3 + \mathcal{C}_3) + \cdots], \tag{A4}$$

where the symbol $\cdots$ stands for higher-order terms. The coefficients for a_s^2 and higher orders should vanish, which leads to

$$r_1 = -\mathcal{C}_1, \tag{A5}$$

$$r_2 = 2\mathcal{C}_1^2 - \mathcal{C}_2, \tag{A6}$$

$$r_3 = \mathcal{C}_1^3 - 3(2\mathcal{C}_1^2 - \mathcal{C}_2)\mathcal{C}_1 + 2\mathcal{C}_1\mathcal{C}_2 - \mathcal{C}_3$$
$$\vdots \tag{A7}$$

As a further step, we introduce a new function

$$\mathcal{R}(Q) = \frac{\partial}{\partial \ln Q^2}\varrho_n(Q) = 4\beta^{\mathcal{R}}\frac{\partial}{\partial a_s(Q)}\varrho_n(Q), \tag{A8}$$

where Q is the scale at which the observable is measured. Since ϱ_n and Q are physical quantities, $\mathcal{R}$ can also be regarded as a physical quantity that does not depend on the renormalization scheme and scale. Equation (A8) can be expanded over ϱ_n in the following form:

$$\mathcal{R} = -\varrho_n^2[4b_0 + 4\varrho_n(2r_1b_0 + b_1 + 2\mathcal{C}_1b_0) + 4\varrho_n^2(r_1^2b_0 + 3r_1b_1 + 6r_1b_0\mathcal{C}_1 + 2r_2b_0 + b_2 + 3b_0\mathcal{C}_2 + 2b_1\mathcal{C}_1) + 4\varrho_n^3(2r_1r_2b_0 + 2r_3b_0 + 3r_1^2b_1 + 3r_2b_1 + 4r_1b_2 + b_3 + 6r_1^2b_0\mathcal{C}_1 + 6r_2b_0\mathcal{C}_1 + 8r_1b_1\mathcal{C}_1 + 2b_2\mathcal{C}_1 + 12r_1b_0\mathcal{C}_2 + 3b_1\mathcal{C}_2 + 4b_0\mathcal{C}_3) + \cdots] \tag{A9}$$

$$= -\varrho_n^2[4b_0 + 4\varrho_n b_1 + 4\varrho_n^2(b_2 - b_0\mathcal{C}_1^2 - b_1\mathcal{C}_1 + b_0\mathcal{C}_2) + 4\varrho_n^3(4b_0\mathcal{C}_1^3 - 6b_0\mathcal{C}_1\mathcal{C}_2 + 2b_0\mathcal{C}_3 + b_1\mathcal{C}_1^2 - 2b_2\mathcal{C}_1 + b_3) + \cdots]. \tag{A10}$$

Both ϱ_n and $\mathcal{R}$ are physical quantities; the expansion coefficients of $\mathcal{R}$ over ϱ_n should be RG invariants. Transforming these RG-invariant coefficients back into the notation used in the body of the text, we get the RG invariants ρ_n ($n > 1$). The first two are

$$\rho_2 = \frac{\beta_2}{16\beta_0} - \frac{\beta_1\mathcal{C}_1}{4\beta_0} - \mathcal{C}_1^2 + \mathcal{C}_2, \tag{A11}$$

$$\rho_3 = \frac{\beta_3}{64\beta_0} + \frac{\beta_1\mathcal{C}_1^2}{4\beta_0} - \frac{\beta_2\mathcal{C}_1}{8\beta_0} + 4\mathcal{C}_1^3 - 6\mathcal{C}_2\mathcal{C}_1 + 2\mathcal{C}_3. \tag{A12}$$

Finally, by replacing ϱ_n with $\varrho_n^{\frac{1}{p}}$, we can obtain the RG invariants for any p, the first two of which agree with Eqs. (22) and (24).

[1] E. C. G. Stuckelberg and A. Peterman, Helv. Phys. Acta **X**, Suppl., XX **26**, 499 (1953).
[2] M. Gell-Mann and F. E. Low, Phys. Rev. **95**, 1300 (1954).
[3] N. N. Bogoliubov and D. V. Shirkov, Dokl. Akad. Nauk SSSR **103**, 391 (1955).
[4] C. G. Callan, Phys. Rev. D **2**, 1541 (1970).
[5] K. Symanzik, Commun. Math. Phys. **18**, 227 (1970).
[6] A. Peterman, Phys. Rep. **53**, 157 (1979).
[7] X. G. Wu, S. J. Brodsky, and M. Mojaza, Prog. Part. Nucl. Phys. **72**, 44 (2013).
[8] P. M. Stevenson, Phys. Rev. D **23**, 2916 (1981).
[9] P. M. Stevenson, Phys. Lett. **100B**, 61 (1981).
[10] P. M. Stevenson, Nucl. Phys. **B203**, 472 (1982).
[11] J. Chyla, A. L. Kataev, and S. A. Larin, Phys. Lett. B **267**, 269 (1991).
[12] S. G. Gorishnii, A. L. Kataev, S. A. Larin, and L. R. Surguladze, Phys. Rev. D **43**, 1633 (1991).

[13] X. G. Wu, Y. Ma, S. Q. Wang, H. B. Fu, H. H. Ma, S. J. Brodsky, and M. Mojaza, arXiv:1405.3196.
[14] A. C. Mattingly and P. M. Stevenson, Phys. Rev. D **49**, 437 (1994).
[15] P. M. Stevenson, Nucl. Phys. **B875**, 63 (2013).
[16] S. J. Brodsky and X. G. Wu, Phys. Rev. D **86**, 054018 (2012).
[17] G. Kramer and B. Lampe, Z. Phys. C **39**, 101 (1988).
[18] G. Kramer and B. Lampe, Z. Phys. A **339**, 189 (1991).
[19] A. P. Contogouris and N. Mebarki, Phys. Rev. D **39**, 1464 (1989).
[20] P. M. Stevenson, Nucl. Phys. **B868**, 38 (2013).
[21] P. A. Baikov, K. G. Chetyrkin, and J. H. Kuhn, Phys. Lett. **101B**, 012002 (2008).
[22] P. A. Baikov, K. G. Chetyrkin, and J. H. Kuhn, Nucl. Phys. B, Proc. Suppl. **189**, 49 (2009).
[23] P. A. Baikov, K. G. Chetyrkin, and J. H. Kuhn, Phys. Rev. Lett. **96**, 012003 (2006).
[24] P. A. Baikov and K. G. Chetyrkin, Phys. Rev. Lett. **97**, 061803 (2006).
[25] S. J. Brodsky, G. P. Lepage, and P. B. Mackenzie, Phys. Rev. D **28**, 228 (1983).
[26] S. J. Brodsky and X. G. Wu, Phys. Rev. D **85**, 034038 (2012).
[27] S. J. Brodsky and X. G. Wu, Phys. Rev. D **85**, 114040 (2012).
[28] S. J. Brodsky and X. G. Wu, Phys. Rev. D **86**, 014021 (2012).
[29] S. J. Brodsky and X. G. Wu, Phys. Rev. Lett. **109**, 042002 (2012).
[30] S. J. Brodsky and L. D. Giustino, Phys. Rev. D **86**, 085026 (2012).
[31] M. Mojaza, S. J. Brodsky, and X. G. Wu, Phys. Rev. Lett. **110**, 192001 (2013).
[32] S. J. Brodsky, M. Mojaza, and X. G. Wu, Phys. Rev. D **89**, 014027 (2014).
[33] S. J. Brodsky and H. J. Lu, Phys. Rev. D **51**, 3652 (1995).
[34] H. D. Politzer, Phys. Rev. Lett. **30**, 1346 (1973).
[35] D. Gross and F. Wilczek, Phys. Rev. Lett. **30**, 1343 (1973).
[36] O. V. Tarasov, A. A. Vladimirov, and A. Yu Zharkov, Phys. Lett. **93B**, 429 (1980).
[37] S. A. Larin and J. A. M. Vermaseren, Phys. Lett. B **303**, 334 (1993).
[38] T. van Ritbergen, J. A. M. Vermaseren, and S. A. Larin, Phys. Lett. B **400**, 379 (1997).
[39] K. G. Chetykin, Nucl. Phys. **B710**, 499 (2005).
[40] M. Czakon, Nucl. Phys. **B710**, 485 (2005).
[41] D. J. Gross and A. Neveu, Phys. Rev. D **10**, 3235 (1974).
[42] B. Lautrup, Phys. Lett. **69B**, 109 (1977).
[43] R. Shrock, Phys. Rev. D **88**, 036003 (2013)
[44] R. Shrock, Phys. Rev. D **90**, 045011 (2014).
[45] G. Choi and R. Shrock, Phys. Rev. D **90**, 125029 (2014).
[46] H. J. Lu and S. J. Brodsky, Phys. Rev. D **48**, 3310 (1993).
[47] P. M. Stevenson, Phys. Rev. D **33**, 3130 (1986).
[48] A. C. Mattingly and P. M. Stevenson, Phys. Rev. Lett. **69**, 1320 (1992).
[49] A. C. Mattingly and P. M. Stevenson, Phys. Rev. D **49**, 437 (1994).
[50] K. A. Olive *et al.* (Particle Data Group). Chin. Phys. C **38**, 090001 (2014).
[51] Y. Ma *et al.* (to be published).
[52] P. M. Stevenson, Nucl. Phys. **B231**, 65 (1984).
[53] W.E. Caswell, Ann. Phys. (Berlin) **123**, 153 (1979).
[54] R. Marshall, Z. Phys. C **43**, 595 (1989).
[55] C. S. Lam and T. M. Yan, Phys. Rev. D **16**, 703 (1977).
[56] E. Braaten, Phys. Rev. D **39**, 1458 (1989).
[57] K. Ackerstaff *et al.* (OPAL Collaboration), Eur. Phys. J. C **7**, 571 (1999).
[58] K. G. Chetyrkin, Phys. Lett. B **390**, 309 (1997).
[59] K. G. Chetyrkin and M. Steinhauser, Phys. Lett. B **408**, 320 (1997).
[60] S. Q. Wang, X. G. Wu, X. C. Zheng, J. M. Shen, and Q. L. Zhang, Eur. Phys. J. C **74**, 2825 (2014).
[61] S. Q. Wang, X. G. Wu, X. C. Zheng, G. Chen, and J. M. Shen, J. Phys. G **41**, 075010 (2014).
[62] S. Q. Wang, X. G. Wu, J. M. Shen, H. Y. Han, and Y. Ma, Phys. Rev. D **89**, 116001 (2014).
[63] S. Q. Wang, X. G. Wu, and S. J. Brodsky, Phys. Rev. D **90**, 037503 (2014).
[64] S. Q. Wang, X. G. Wu, Z. G. Si, and S. J. Brodsky, Phys. Rev. D **90**, 114034 (2014).
[65] G. Grunberg, Phys. Lett. **95B**, 70 (1980); **110B**, 501 (1982).
[66] G. Grunberg, Phys. Rev. D **29**, 2315 (1984).
[67] C. J. Maxwell, Phys. Rev. D **29**, 2884 (1984).